Available online at website: https://journal.bcrec.id/index.php/bcrec

Bulletin of Chemical Reaction Engineering & Catalysis, 19 (2) 2024, 275-284

Research Article

Conversion of Isopropanol to Diisopropyl Ether over Cobalt Phosphate Modified Natural Zeolite Catalyst

Hasanudin Hasanudin [1,2*], Wan Ryan Asri [1,2], R. Rahmawati [1,2], Fahma Riyanti [1,2], Roni Maryana [3], Muhammad Al Muttaqii [3], Nino Rinaldi [3], Fitri Hadiah [4], N. Novia [4]

[1]Department of Chemistry, Faculty of Mathematics and Natural Science, Universitas Sriwijaya, Inderalaya 30662, South Sumatra, Indonesia.
[2]Biofuel Research Group, Faculty of Mathematics and Natural Science, Universitas Sriwijaya, Inderalaya 30662, South Sumatra, Indonesia.
[3]Research Center for Chemistry, National Research and Innovation Agency, Building 452 KST BJ Habibie, Serpong Tangerang Selatan, Banten, Indonesia.
[4]Department of Chemical Engineering, Faculty of Engineering, Unviersitas Sriwijaya, Indralaya 30662, Indonesia.

Received: 13th April 2024; Revised: 3rd June 2024; Accepted: 4th June 2024
Available online: 17th June 2024; Published regularly: August 2024

Abstract

This study aims to produce diisopropyl ether (DIPE) via isopropanol dehydration using cobalt-phosphate-supported natural zeolite catalysts. The catalytic activities of the zeolite/CoO and zeolite/$Co(H_2PO_4)_2$ were compared. The as-prepared catalysts were assessed using X-ray diffraction (XRD), scanning electron microscopy (SEM) with energy-dispersive X-ray spectroscopy (EDX), Fourier transform infrared (FTIR) spectroscopy, and N_2 adsorption-desorption. Surface acidity was determined using the gravimetric method with pyridine as the probe. The results of this study showed that natural zeolite was favorably impregnated by CoO and $Co(H_2PO_4)_2$ species. The impregnation process affected the textural and acidic features of the catalysts. The zeolite/$Co(H_2PO_4)_2$ catalyst with a loading of 8 $mEq.g^{-1}$ exhibited the highest surface acidity of 1.827 $mmol.g^{-1}$. This catalyst also promoted the highest catalytic activity towards isopropanol dehydration, with an isopropanol conversion of 66.19%, DIPE selectivity, and yield of 46.72% and 34.99%, respectively. The cobalt phosphate species promoted higher catalytic activity for isopropanol dehydration than the CoO species. This study demonstrated the potential of cobalt phosphate-supported natural zeolite catalysts for DIPE production with adequate performance.

Keywords: isopropanol dehydration; diisopropyl ether; natural zeolite; cobalt phosphate; impregnation

How to Cite: H. Hasanudin, W.R. Asri, R. Rahmawati, F. Riyanti, R. Maryana, M. Al Muttaqii, N. Rinaldi, F. Hadiah, N. Novia (2024). Conversion of Isopropanol to Diisopropyl Ether over Cobalt Phosphate Modified Natural Zeolite Catalyst. *Bulletin of Chemical Reaction Engineering & Catalysis*, 19 (2), 275-284 (doi: 10.9767/bcrec.20144)

Permalink/DOI: https://doi.org/10.9767/bcrec.20144

1. Introduction

It is well known that the majority of automobiles in use presently are powered by fossil fuels. Air pollution from vehicles and industries has become one of the most critical issues in recent years, particularly in large cities. The use of alternative fuels is an effective strategy to replace fossil fuels and reduce air pollution. Various additives have been added to fuels to ensure quality, local, and clean fuels for motor vehicles, while reducing vehicle emissions. Currently, ether compounds, such as methyl tertiary butyl ether (MTBE), are widely used as gasoline additives [1]. However, prolonged exposure to MTBE is known to cause eye irritation, health risks, and headaches owing to its carcinogenic properties. On the other hand, diisopropyl ether (DIPE) is used in various applications, including fuel additives, synthesis intermediates, and organic solvents. DIPE can replace MTBE as an additive fuel, increasing the octane number and improving

* Corresponding Author.
Email: hasanudin@mipa.unsri.ac.id (H. Hasanudin)

combustion conditions owing to its higher oxygen content and better compatibility [2].

Currently, DIPE production has been extensively explored using various methods and operating conditions. In this regard, isopropanol can be employed as a raw material for synthesizing DIPE as an environmentally friendly precursor and a cost-effective procedure [3,4]. Armenta *et al*. [5] reported that an adequate acidic site on a solid catalyst would promote the dehydration product towards DIPE, whereas basic site of the catalyst leads to propylene formation. The development of catalysts is crucial for achieving an adequate conversion. Heterogeneous acid catalysts are widely used in converting alcohol into ether, as this catalyst exhibits low corrosiveness, is easier to obtain due to low prices, and is easy to separate. Some of the catalysts typically employed in this dehydration method are zeolites, heteropolyacids, bentonite, alumina, zirconia, and titania [6–8]. Zeolite is a promising catalyst because of its unique characteristics, such as thermal and chemical stability, Lewis and Brønsted acid sites [9], homogeneous pore size distribution, and shape selectivity [5].

Numerous studies have been conducted to modulate the physicochemical properties of zeolites for various potential applications [10]. Several species, such as phosphomolybdic acid [11], Cu and Fe [12], Ni [13–15], Fe/Al [16], Ni-Mo, Co, Co-Mo [17], and Co [18], have been extensively combined with zeolites for multifunctional purposes. The impregnation of transitional metal species into zeolites enlarges the pore structure and enhances their acidity, thus promoting effective catalytic activity [19]. Currently, metal phosphate-based materials have enhanced recognition and have also been utilized as heterogeneous acid catalysts for catalytic dehydration owing to the coexistence of moderately strong Lewis acid sites (metal species) and Brønsted acids (protonated phosphoric groups) [20]. Cobalt phosphate (CoP) is a promising metal phosphate for use in catalytic reactions. Cobalt phosphate-based compounds are inexpensive, abundantly available, more sustainable, environmentally friendly, and comparable to noble metal-based catalysts [21]. The potential of cobalt phosphates as an oxygen evolution-reduction catalyst has been extensively studied [22–27], revealing a remarkable catalytic performance. However, cobalt phosphate is rarely used in alcohol dehydration reactions. As mentioned earlier, a typical transition-metal-supported catalyst is very intriguing for the catalysis process. In this context, the fabrication of cobalt phosphate-natural zeolite has a potential synergetic effect on isopropanol dehydration because both catalysts exhibit sufficient catalytic features. This modification could also promote the potential of low-cost natural zeolites as suitable support catalysts.

To the best of our knowledge, the dehydration of isopropanol to DIPE using CoP/zeolite catalysts has not been sufficiently explored. This research investigates the effect of cobalt phosphate loading on the catalytic activity towards isopropanol conversion to DIPE compared with uncontained phosphor Co-zeolite. The physicochemical properties of the catalysts were evaluated using a series of characterizations such as XRD, SEM-EDX, FTIR, and N_2 gas sorption, as well as their total acidity features using the gravimetric method.

2. Materials and Methods

2.1 Zeolite Preparation

Bulky natural zeolite (Lampung) was ground with a mortar grinder to obtain a homogeneous powder that passed through a 200-mesh sieve. The resulting zeolite powder was then dried at 120 °C for 3 h. Subsequently, 200-mesh natural zeolite (100 g) was soaked in a 1% HF solution and stirred for 1 h and 6 N HCl solutions for 4 h. The resulting powder was filtered and washed with distilled water until the pH was neutral.

2.2 Imprenagnation of Cobalt Phosphate to Dealuminated Natural Zeolite

Briefly, the as-prepared natural zeolite (5 g) was dispersed in a 0.1 M $CoCl_2.6H_2O$ solution (Merck) and subsequently stirred for 1 h at ambient temperature. Then, a 0.1 M $NH_4H_2PO_4$ solution (Merck) was gradually introduced (1 $mL.min^{-1}$) until it reached a concentration of 2, 4, 6, 8, and 10 $mEq.g^{-1}$ of cobalt phosphate loading and stirred at room temperature for 5 h. The temperature increased to 80 °C until a paste formed. The resulting paste was washed with distilled water, dried at 105 °C, and calcinated at 350 °C for 4 h under an oxygen atmosphere. The as-prepared catalyst was denoted as zeolite/$Co(H_2PO_4)_2$. Zeolite/CoO was prepared as a control.

2.3 Characterization of Catalyst

Zeolite/CoO and zeolite/$Co(H_2PO_4)_2$ were analyzed using XRD (Rigaku Minu Flex 600) to determine the crystal structure of the catalyst using Cu-Kα radiation (λ = 1.54056 Å). X-ray tubes were operated at 40 kV and 30 mA. The surface and elemental composition of the catalyst were analyzed using SEM-EDX (JSM 6510). The Brunauer–Emmett–Teller (BET) method was employed to analyze the surface area over a gas sorption analyzer. The pore size and pore volume were calculated using the BJH method. The functional groups of both catalysts were analyzed using a Shimadzu FTIR 8201 instrument.

Measurements were carried out at wavenumbers ranging from 1400 to 1600 cm^{-1}. The surface acidity of the catalysts was calculated using the gravimetric method with pyridine as a probe in a desiccator. Before the analysis, the desiccator was vacuumed for 1 h, and the catalyst (0.5 g) was dried in an oven at 100 ˚C.

2.4 Isopropanol Dehydration

Initially, 50 mL of isopropanol (Merck) was added to a round flask, followed by the addition of 5 g of the catalyst. The reaction was conducted using a reflux system equipped with an oil bath and thermometer. The round flask was placed in a container filled with oil and refluxed for 3.5 h at 150 °C. The product and catalyst were filtered at room temperature, and the product was measured using GC-MS (Thermo Fisher Scientific). Regarding the quantification of the organic molecule, we utilized TG-5-MS columns for GC-MS analysis. The starting oven programmed temperature was 32 ˚C for 2.5 mins and escalated at 3 C˚ min^{-1} to a final temperature of 45 ˚C for 2 mins, with He as the carrier gas (1 $mL.min^{-1}$). The injection temperature was 200 ˚C. MS transfer line temperature was 230 ˚C, whereas the ion source temperature was 210 ˚C.

The activities of the catalysts were determined using Eqs. (1)– (3) as follows:

$$Conversion_{isopropanol} = \frac{Init.mole_{isopropanol} - Final\ mole_{isopropanol}}{Init.\ mole_{isopropanol}} x100\% \quad (1)$$

$$Yield_{Diisopropyl\ ether} = \frac{Product\ mole_{Diisopropyl\ ether} \times 2}{Init.\ mole_{isopropanol} - Final\ mole_{isopropanol}} x100\% \quad (2)$$

$$Selectivity_{Diisopropyl\ ether} = \frac{Product\ mole_{Diisopropyl\ ether} \times 2}{Init.\ mole_{isopropanol}} x100\% \quad (3)$$

3. Results and Discussion

3.1 Catalyst Characterizations

The XRD diffractograms of the natural zeolite, zeolite/CoO, and zeolite/$Co(H_2PO_4)_2$ are shown in Figure 1. It can be seen that the natural zeolite revealed 2θ peaks at 11.21, 13.45, and 23.15◦ were assigned as mordenite phase (JCPDS No. 47-1870), whereas 2θ peaks at 22.21, 25.60, and 27.56◦ corresponded to the clinoptilolite phases (JCPDS No. 06-0239) [28]. These phases were also observed in the diffractogram of zeolite/CoO (Figure 1b) at 2θ = 13.45, 22.26, 25.60, and 27.5°, as well as on zeolite/$Co(H_2PO_4)_2$ at 2θ of 13.36, 22.22, 25.69, and 27.85°, which indicated that the main zeolite phase was still maintained after loading with CoO and $Co(H_2PO_4)_2$, respectively. The relative shift on 2θ occurred due to the impregnation method's effect, resulting in stress owing to the difference in ionic size on the Co, CoP, and the parent zeolite [29]. Furthermore, the Co and CoP phases are relatively indistinguishable, presumably due to the particle being evenly dispersed on the zeolite with a low concentration [30,31].

Micrographs of the surface morphologies of the catalysts are shown in Figure 2. The SEM micrographs of natural zeolite (Figure 2a-b) revealed a uniform surface and smoothness, consistent with previous reports [32]. Mehdi *et al.* [33] reported that natural zeolites usually had curvy and coarse surfaces. The zeolite/CoO (Figure 2c) had a non-uniform layered surface shape, which suggests that the Co species were successfully impregnated into the zeolite [34]. No appreciable surface morphological changes were observed in zeolite/$Co(H_2PO_4)_2$ compared to the zeolite/CoO catalyst (Figure 2d). However, the morphology of the surface appeared uneven, presumably because of the effect of the $Co(H_2PO_4)_2$ species. There were no sizeable cobalt or cobalt phosphate species on the surface of the catalyst, which suggested that these species were effective in being employed with a supported catalyst [35].

The EDX spectra of all catalysts are presented in Figure 3. The catalysts consisted of Si, Al, Co, P, and other impurities. According to the semiquantitative analysis, there was an appreciable increase in the Co content after zeolite modification from 0 to 2.23% and 1.61% for zeolite/CoO and zeolite/$Co(H_2PO_4)$, respectively, which indicated that the impregnation of Co species into the zeolite was successfully achieved. Moreover, the phosphorus content of 9.23% in the zeolite/$Co(H_2PO_4)$ catalyst suggested that the

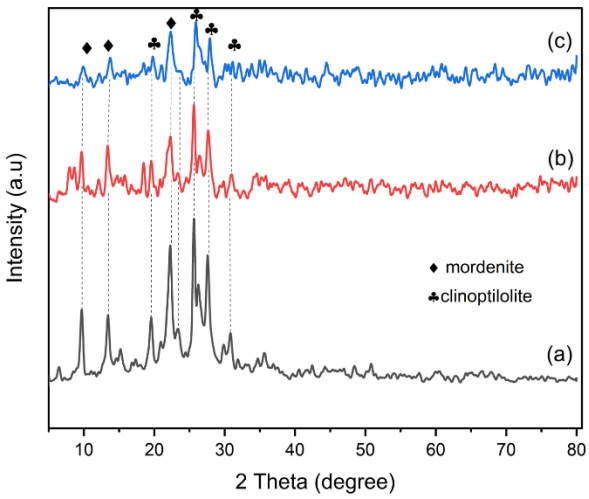

Figure 1. X-ray diffractogram of (a) Natural zeolite, (b) Zeolite/CoO and (c) Zeolite/$Co(H_2PO_4)_2$.

cobalt phosphate species had been favorably introduced into the zeolite framework.

The FTIR spectra of the catalysts are shown in Figure 4. It can be seen that the bands at 950–1250 cm^{-1} were identified as stretching vibrations of the Si(Al)–O bonds of zeolite [36]. The absorption peaks at ca. 745-700 cm^{-1} were attributed to the symmetric SiO_4 stretching vibration [37]. The bands at ca. 457.13 and 582.50 cm^{-1} was observed for all the catalysts, indicating the presence of Si–O–Si bonds. Cobalt species appeared in bands ranging from 600-400 cm^{-1} [39-38]. However, the P–O and Co–O functional groups were relatively unobserved, presumably because of the overlap between the alumina-silicate framework and cobalt species.

The acidity of the catalyst is a crucial aspect of the catalytic reaction. Because pyridine is an aromatic Lewis base that can serve as a proton acceptor from the alumina-silicate surface, it is a more stringent diagnostic tool for solid surface acidity [40]. After pyridine adsorption in the gas phase, the acid sites on the catalyst surface (Brønsted or Lewis acid) were qualitatively evaluated by FTIR. The type of acid site is governed by the surface protons that lead to Brønsted sites or cationic centers, such as Lewis sites, through coordination bond interactions [41]. Figure 4c appeared the band at 1637.56-1641.42 cm^{-1} indicating the Brønsted sites [42], whereas the characteristic of Lewis sites related to bands ranging from 1440.83-1436.97 cm^{-1} as shown in Figure 4c [18].

The surface acidities of zeolite, zeolite/CoO, and zeolite/$Co(H_2PO_4)_2$ obtained using the gravimetric method are presented in Table 1. The parent zeolite had a low acidity value, which increased after being loaded with the Co species. Moreover, it can be seen that the addition of phosphate species to the cobalt dramatically increased the catalyst's surface acidity. This increase corresponded to an increase in the number of Brønsted acid sites derived from the phosphate groups [20,43]. The cobalt phosphate species generated highly acidic sites, which increased the surface acidity of the catalyst.

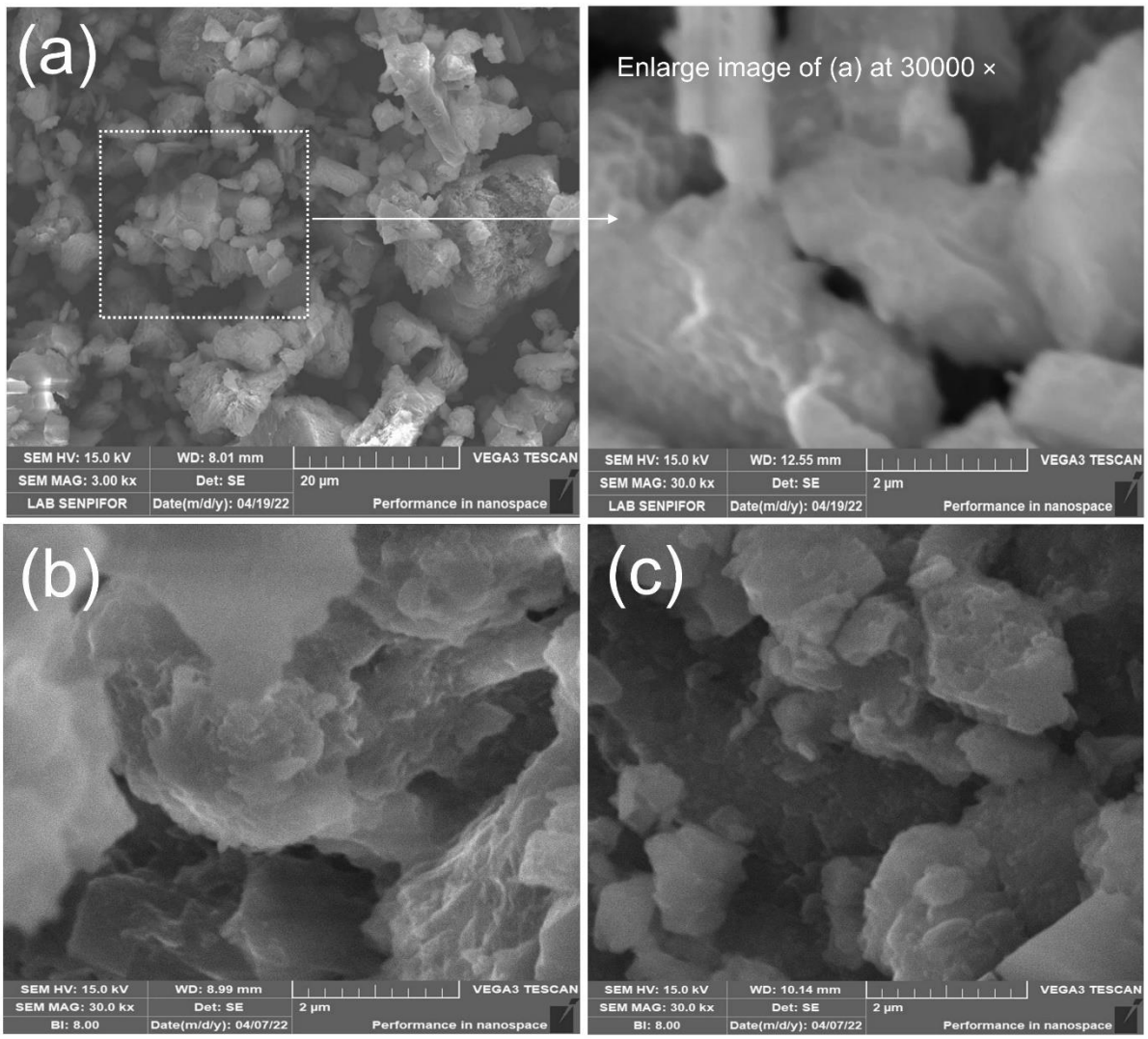

Figure 2. Representative SEM micrographs of (a) natural zeolite (b) Zeolite/CoO, (c) Zeolite/$Co(H_2PO_4)_2$

Moreover, prolonged cobalt phosphate loading up to 8 mEq.g^{-1} increased the surface acidity of zeolite/Co$(H_2PO_4)_2$ to 1.827 mmol pyridine.g^{-1}. A similar trend was also consistently reported in another study [44]. Meanwhile, high cobalt loading (10 mEq.g^{-1}) decreased the surface acidity of the catalyst. The decrease in surface acidity could be due to the agglomeration of the catalyst; thus, pyridine adsorption did not take place effectively [45].

The N_2 adsorption-desorption isotherms and the pore size distribution of the catalysts are presented in Figure 5. All the catalysts exhibited type IV behavior, indicating that the catalysts were mesoporous. A hysteresis curve was observed for all catalysts, denoted as type H4, which suggested that the catalysts had slit-shaped pores [46]. According to Li *et al*. [47], this textural feature is related to the presence of cylindrical pores. The large pores could promote

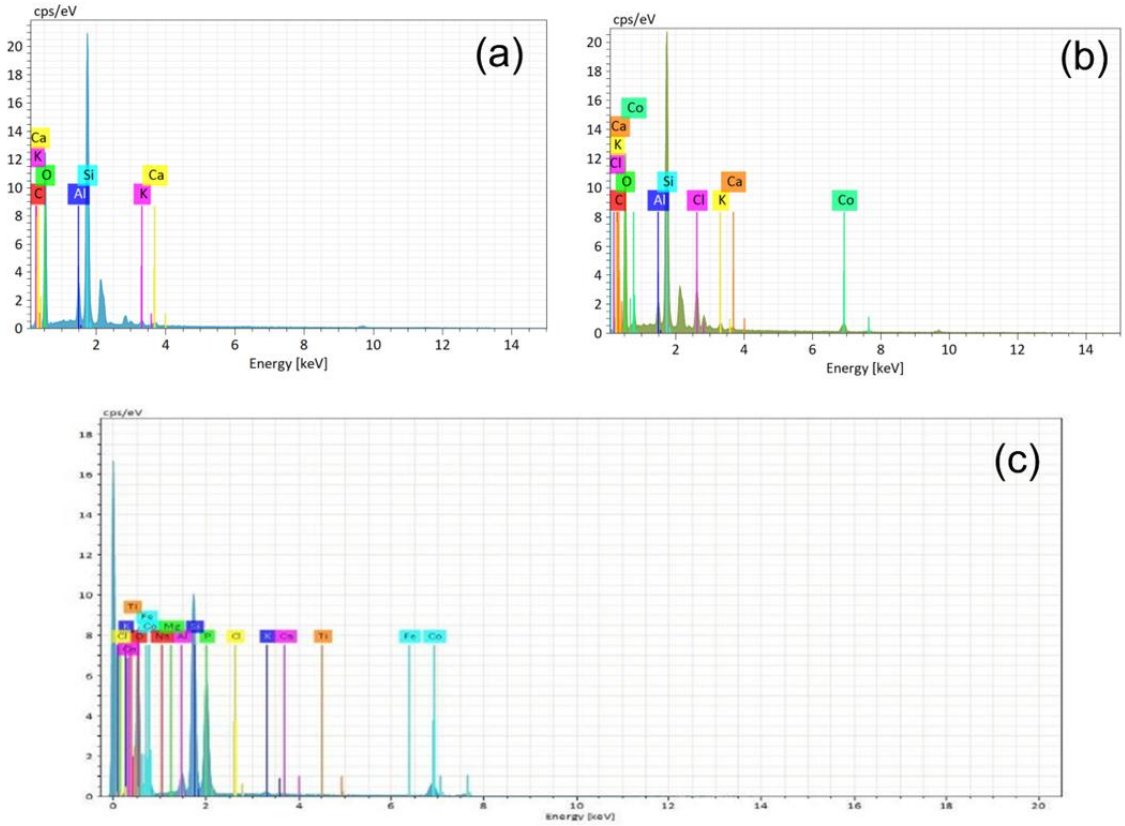

Figure 3. EDX spectra for (a) Natural zeolite (b) Zeolite/Co, and (c) Zeolite/Co$(H_2PO_4)_2$

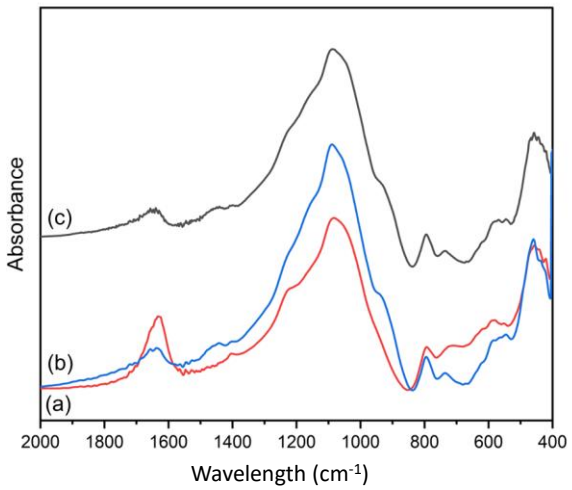

Figure 4. FTIR spectra for (a) Zeolite/CoO (b) Zeolite/Co$(H_2PO_4)_2$, and (c) Zeolite/Co$(H_2PO_4)_2$-pyridine absorbed

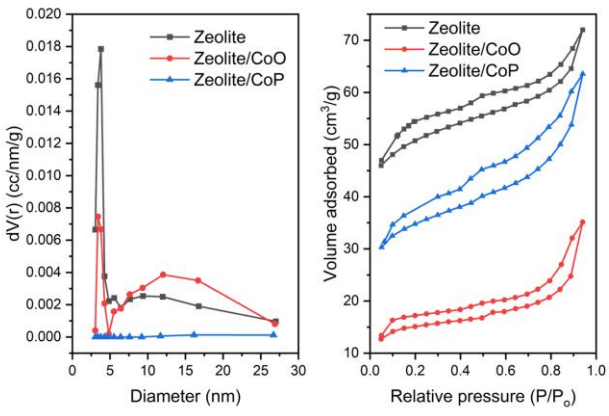

Figure 5. N_2 physisorptions and pore size distribution of natural zeolite, zeolite/Co, and zeolite//Co$(H_2PO_4)_2$

the rapid diffusion of reactants as well as products.

The BET surface areas and porosities of the catalysts are presented in Table 2. It was revealed that impregnation of the zeolite with CoO species decreased the surface area from 135.1 to 47.9 $m^2.g^{-1}$. Meanwhile, the pore size and volume decreased as well to 16.06 nm and 0.05 $cm^3.g^{-1}$, respectively. These results indicate that the pores of the zeolite are blocked by the CoO species, resulting in a decrease in the surface area [48]. Higher decreases in surface area (30.1 $m^2.g^{-1}$) and porosity with a pore size of 14.17 nm and pore volume of 0.04 $cm^3.g^{-1}$, were observed in the zeolite-$Co(H_2PO_4)_2$ catalyst. The decrease in the surface area of zeolite-$Co(H_2PO_4)_2$ was higher than that of the zeolite/CoO counterparts.

3.2 Isopropanol Dehydration Conversion

The conversion of isopropanol to DIPE was conducted under reflux at 150 ˚C for 3.5 hours using 5 g of the catalyst and 50 mL of isopropropanol. The catalytic activities of zeolite/CoO and zeolite/$Co(H_2PO_4)$ with various cobalt phosphate loadings towards the DIPE product as well as the conversion are presented in Table 3. The parent zeolite catalyst exhibited low catalytic activity towards isopropanol dehydration owing to its low acidity. Meanwhile, zeolite/CoO promoted 46.10% conversion towards isopropanol, with a DIPE selectivity of 23.63% and a yield of 1.78% with no side products. zeolite/$Co(H_2PO_4)$ with 2 $mEq.g^{-1}$ loadings promoted high DIPE selectivity and yield of up to 31.36% and 23.50%, respectively. This indicated that the phosphorous species enhanced the catalytic activity of the zeolite to a high DIPE product. Furthermore, the higher loading of cobalt phosphate gradually increased the DIPE yield and selectivity, which suggested that the acidity of the catalyst likely affected the catalyst performance during the dehydration process [5]. Meanwhile, the surface acidity of the catalyst was not correlated with the isopropanol conversion. The textural features of the catalyst might affect its catalytic activity, suggesting that a small pore size and volume might positively enhance the selectivity and yield of the DIPE product [49]. No appreciable catalytic activity was observed for zeolite/$Co(H_2PO_4)$ under high cobalt phosphate loading. Higher catalyst loading could result in the formation of aggregates or lumps, which causes dehydration to be inadequate [50]. Turek *et al*. [51] reported that γ-Al_2O_3 exhibited 12.1% of DIPE selectivity at a temperature of 500 K, whereas $H_3PMo_{12}O_{40}$ showed higher DIPE selectivity (31.5%). [52] showed that combined silica-zirconia (20-30 mol %) provided 5-13% DIPE selectivity and 10-50% of isopropanol conversion at a temperature of 180-210 ˚C. Compared with other zeolite-based catalysts, zeolite/NiP (8 $mEq.g^{-1}$) exhibited high isopropanol conversion (66.73%), with DIPE selectivity and yield of 47.8% and 35.81%, respectively [53]. Compared with previous

Table 1. Total acidity results of catalysts using the gravimetric method.

Sample	Total acidity ($mmol.g^{-1}$)
Zeolite	0.102
Zeolite/CoO	0.183
Zeolite/$Co(H_2PO_4)_2$ 2 mEq/g	0.767
Zeolite/$Co(H_2PO_4)_2$ 4 mEq/g	0.802
Zeolite/$Co(H_2PO_4)_2$ 6 mEq/g	1.334
Zeolite/$Co(H_2PO_4)_2$ 8 mEq/g	1.827
Zeolite/$Co(H_2PO_4)_2$ 10 mEq/g	1.378

Table 2. S_{BET} and porosity analysis of catalysts

Catalyst	Surface area ($m^2.g^{-1}$)	Pore size (nm)	Pore volume ($cm^3.g^{-1}$)
Natural zeolite	135.1	17.01	0.11
Zeolite/CoO	47.9	16.06	0.05
Zeolite/$Co(H_2PO_4)_2$	30.1	14.17	0.04

Table 3. Isopropanol conversion, selectivity, and yield of DIPE catalyzed by various catalysts at T = 150 ˚C, *t* = 3.5 h, catalyst = 5 g, isopropropanol = 50 mL

Catalysts	Isopropanol conversion (%)	DIPE Selectivity (%)	DIPE Yield (%)
Zeolite	10.23	13.23	0.21
Zeolit/CoO	46.10	23.63	1.78
Zeolite/$Co(H_2PO_4)_2$ 2 mEq/g	16.38	31.36	23.50
Zeolite/$Co(H_2PO_4)_2$ 4 mEq/g	57.80	41.51	30.83
Zeolite/$Co(H_2PO_4)_2$ 6 mEq/g	54.98	43.66	32.90
Zeolite/$Co(H_2PO_4)_2$ 8 mEq/g	66.19	46.72	34.99
Zeolite/$Co(H_2PO_4)_2$ 10 mEq/g	50.45	45.99	36.20

reports, this study indicated that the zeolite/CoP catalyst has sufficient catalytic activity towards the DIPE product, which might possibly be scaled up for industrial use. To fully comprehend the catalytic process, however, more studies regarding the impact of experimental variables, such as temperature, catalyst weight, and time reaction, must be undertaken. In addition, further study regarding the reusability of the catalysts should be evaluated to determine their DIPE production stability throughout consecutive runs.

4. Conclusions

In summary, natural zeolite catalysts were impregnated using CoO and cobalt phosphate at various loading of 2-10 $mEq.g^{-1}$. The catalytic activities of these catalysts were explored for the dehydration of isopropanol to DIPE. Based on the results of catalyst characterization, it was shown that the impregnation process had been successfully achieved. The natural zeolite properties were successfully enhanced by the Co and $Co(H_2PO_4)_2$ species, leading to the increase in the catalytic activity towards isopropanol dehydration to DIPE. The catalytic study revealed that zeolite-$Co(H_2PO_4)_2$ with 8 $mEq.g^{-1}$ loading had the highest selectivity and yield of DIPE, as well as isopropanol conversion, accompanied by high surface acidity compared with zeolite/CoO. This study demonstrates the potential application of a cobalt phosphate-based catalyst supported with natural zeolite as a low-cost supported catalyst for isopropanol dehydration, which might possibly be scaled up for industrial use.

Acknowledgment

The authors acknowledge The Biofuel Research Group, Faculty of Mathematics and Natural Science, Universitas Sriwijaya, for providing the research apparatus. The instrumental characterization was supported by the Badan Riset dan Inovasi Nasional (BRIN), and the fruitful discussions were thoroughly recognized.

Credit Author Statement

Author Contributions: H. Hasanudin: Conceptualization, Writing, Review and Editing, Supervision; W.R. Asri: Conceptualization, Methodology, Writting Draft Preparation; R. Rahmawati: Data Curation, Methodology; F. Riyanti: Formal Analysis, Data Curation; R. Maryana: Formal Analysis, Data Curation; M. Al Muttaqii: Formal Analysis, Data Curation; Software; N. Rinaldi: Resources, Data Curation; Visualization; F. Hadiah: Data Curation, Validation; N. Novia: Data Curation, Validation. All authors have read and agreed to the published version of the manuscript.

References

[1] Fan, X., Sun, W., Liu, Z., Gao, Y., Yang, J., Yang, B., Law, C.K. (2021). Exploring the oxidation chemistry of diisopropyl ether: Jet-stirred reactor experiments and kinetic modeling. *Proceedings of the Combustion Institute*, 38(1), 321–328. DOI: 10.1016/j.proci.2020.06.242.

[2] Zhang, L., Lim, E.Y., Loh, K.C., Ok, Y.S., Lee, J.T.E., Shen, Y., Wang, C.H., Dai, Y., Tong, Y.W. (2020). Biochar enhanced thermophilic anaerobic digestion of food waste: Focusing on biochar particle size, microbial community analysis and pilot-scale application. *Energy Conversion and Management*, 209(February), 112654. DOI: 10.1016/j.enconman.2020.112654.

[3] Qi, J., Zhu, R., Han, X., Zhao, H., Li, Q., Lei, Z. (2020). Ionic liquid extractive distillation for the recovery of diisopropyl ether and isopropanol from industrial effluent: Experiment and simulation. *Journal of Cleaner Production*, 254, 120132. DOI: 10.1016/j.jclepro.2020.120132.

[4] Murat, M., Tišler, Z., Šimek, J., Hidalgo-Herrador, J.M. (2020). Highly active catalysts for the dehydration of isopropanol. *Catalysts*, 10(6) DOI: 10.3390/CATAL10060719.

[5] Armenta, M.A., Valdez, R., Silva-Rodrigo, R., Olivas, A. (2019). Diisopropyl ether production via 2-propanol dehydration using supported iron oxides catalysts. *Fuel*, 236(April 2018), 934–941. DOI: 10.1016/j.fuel.2018.06.138.

[6] Phung, T.K., Busca, G. (2015). Diethyl ether cracking and ethanol dehydration: Acid catalysis and reaction paths. *Chemical Engineering Journal*, 272, 92–101. DOI: 10.1016/j.cej.2015.03.008.

[7] Zhang, M., Yu, Y. (2013). Dehydration of ethanol to ethylene. *Industrial & Engineering Chemistry Research*, 52 (28), 9505–9514. DOI: 10.1021/ie401157c.

[8] Krutpijit, C., Jongsomjit, B. (2017). Effect of HCl loading and ethanol concentration over HCl-activated clay catalysts for ethanol dehydration to ethylene. *J. Oleo Sci.* DOI: 10.5650/jos.ess17118

[9] Hasanudin, H., Asri, W.R., Meilani, A., Yuliasari, N. (2022). Kinetics Study of Free Fatty Acid Esterification from Sludge Palm Oil Using Zeolite Sulfonated Biochar from Molasses Composite Catalyst. In: *Materials Science Forum*. pp. 113–118. DOI: 10.4028/p-5ovu3d.

[10] Harun, F.W., Almadani, E.A., Radzi, S.M. (2016). Metal cation exchanged montmorillonite K10 (MMT K10): Surface properties and catalytic activity. *Journal of Scientific Research and Development*, 3(3), 90–96.

[11] Gupta, S., Gambhire, A.B., Jain, R. (2022). Conversion of carbohydrates (glucose and fructose) into 5-HMF over solid acid loaded natural zeolite (PMA/NZ) catalyst. *Materials Letters: X*, 13, 100119. DOI: 10.1016/j.mlblux.2021.100119.

[12] Olegario, E.M., Mark Pelicano, C., Cosiñero, H.S., Sayson, L.V., Chanlek, N., Nakajima, H., Santos, G.N. (2021). Facile synthesis and electrochemical characterization of novel metal oxide/Philippine natural zeolite (MOPNZ) nanocomposites. *Materials Letters*, 294, 129799. DOI: 10.1016/j.matlet.2021.129799.

[13] Yao, D., Yang, H., Chen, H., Williams, P.T. (2018). Investigation of nickel-impregnated zeolite catalysts for hydrogen/syngas production from the catalytic reforming of waste polyethylene. *Applied Catalysis B: Environmental*, 227(December 2017), 477–487. DOI: 10.1016/j.apcatb.2018.01.050.

[14] Ferreira, A.D.F., Maia, A.J., Guatiguaba, B., Herbst, M.H., Rocha, P.T.L., Pereira, M.M., Louis, B. (2014). Nickel-doped small pore zeolite bifunctional catalysts: A way to achieve high activity and yields into olefins. *Catalysis Today*, 226, 67–72. DOI: 10.1016/j.cattod.2013.10.033.

[15] Kadarwati, S., Rahmawati, F., Eka Rahayu, P., Wahyuni, S., Imam Supardi, K. (2013). Kinetics and mechanism of Ni/zeolite-catalyzed hydrocracking of palm oil into bio-fuel. *Indonesian Journal of Chemistry*, 13(1), 77–85. DOI: 10.22146/ijc.21330.

[16] Borsella, E., Aguado, R., De Stefanis, A., Olazar, M. Comparison of catalytic performance of an iron-alumina pillared montmorillonite and HZSM-5 zeolite on a spouted bed reactor. *Journal of Analytical and Applied Pyrolysis*, 130, 249–255. DOI: 10.1016/j.jaap.2017.12.015.

[17] Sriningsih, W., Saerodji, M.G., Trisunaryanti, W., Triyono, Armunanto, R., Falah, I.I. (2014). Fuel Production from LDPE Plastic Waste over Natural Zeolite Supported Ni, Ni-Mo, Co and Co-Mo Metals. *Procedia Environmental Sciences*, 20, 215–224. DOI: 10.1016/j.proenv.2014.03.028.

[18] Grzybek, G., Góra-Marek, K., Tarach, K., Pyra, K., Patulski, P., Greluk, M., Słowik, G., Rotko, M., Kotarba, A. (2022). Tuning the properties of the cobalt-zeolite nanocomposite catalyst by potassium: Switching between dehydration and dehydrogenation of ethanol. *Journal of Catalysis*, 407, 364–380. DOI: 10.1016/j.jcat.2022.02.006.

[19] Zhu, J., Wen, K., Zhang, P., Wang, Y., Ma, L., Xi, Y., Zhu, R., Liu, H., He, H. (2017). Keggin-Al30 pillared montmorillonite. *Microporous and Mesoporous Materials*, 242, 256–263. DOI: 10.1016/j.micromeso.2017.01.039.

[20] Ni, W., Li, D., Zhao, X., Ma, W., Kong, K., Gu, Q., Chen, M., Hou, Z. (2019). Catalytic dehydration of sorbitol and fructose by acid-modified zirconium phosphate. *Catalysis Today*, 319 (2010), 66–75. DOI: 10.1016/j.cattod.2018.03.034.

[21] Katkar, P.K., Marje, S.J., Kale, S.B., Lokhande, A.C., Lokhande, C.D., Patil, U.M. (2019). Synthesis of hydrous cobalt phosphate electro-catalysts by a facile hydrothermal method for enhanced oxygen evolution reaction: Effect of urea variation. *CrystEngComm*, 21(5), 884–893. DOI: 10.1039/c8ce01653d.

[22] Shaddad, M.N., Arunachalam, P., Al-Mayouf, A.M., Ghanem, M.A., Alharthi, A.I. (2019). Enhanced photoelectrochemical oxidation of alkali water over cobalt phosphate (Co-Pi) catalyst-modified $ZnLaTaON_2$ photoanodes. *Ionics*, 25(2), 737–745. DOI: 10.1007/s11581-018-2688-y.

[23] Lee, H., Kim, K.H., Choi, W.H., Moon, B.C., Kong, H.J., Kang, J.K. (2019). Cobalt-Phosphate Catalysts with Reduced Bivalent Co-Ion States and Doped Nitrogen Atoms Playing as Active Sites for Facile Adsorption, Fast Charge Transfer, and Robust Stability in Photoelectrochemical Water Oxidation. *ACS Applied Materials and Interfaces*, 11(47), 44366–44374. DOI: 10.1021/acsami.9b16523.

[24] Kim, H., Park, J., Park, I., Jin, K., Jerng, S.E., Kim, S.H., Nam, K.T., Kang, K. (2015). Coordination tuning of cobalt phosphates towards efficient water oxidation catalyst. *Nature Communications*, 6, 1–11. DOI: 10.1038/ncomms9253.

[25] Xuan, L.L., Liu, X.J., Wang, X. (2019). Cobalt phosphate nanoparticles embedded nitrogen and phosphorus-codoped graphene aerogels as effective electrocatalysts for oxygen reduction. *Frontiers in Materials*, 6(February), 1–12. DOI: 10.3389/fmats.2019.00022.

[26] Keane, T.P., Brodsky, C.N., Nocera, D.G. (2019). Oxidative Degradation of Multi-Carbon Substrates by an Oxidic Cobalt Phosphate Catalyst. *Organometallics*, 38(6), 1200–1203. DOI: 10.1021/acs.organomet.8b00337.

[27] Di Palma, V., Zafeiropoulos, G., Goldsweer, T., Kessels, W.M.M., van de Sanden, M.C.M., Creatore, M., Tsampas, M.N. (2019). Atomic layer deposition of cobalt phosphate thin films for the oxygen evolution reaction. *Electrochemistry Communications*, 98(2019), 73–77. DOI: 10.1016/j.elecom.2018.11.021.

[28] Sugiarti, S., Septian, D.D., Maigita, H., Khoerunnisa, N.A., Hasanah, S., Wukirsari, T., Hanif, N., Apriliyanto, Y.B. (2020). Investigation of H-zeolite and metal-impregnated zeolites as transformation catalysts of glucose to hydroxymethylfurfural. *AIP Conference Proceedings*, 2243 (June). DOI: 10.1063/5.0001789.

[29] Valdés, H., Riquelme, A.L., Solar, V.A., Azzolina-Jury, F., Thibault-Starzyk, F. (2021). Removal of chlorinated volatile organic compounds onto natural and Cu-modified zeolite: The role of chemical surface characteristics in the adsorption mechanism. *Separation and Purification Technology*, 258(July 2020), 118080. DOI: 10.1016/j.seppur.2020.118080.

[30] Sharma, A., Lee, B.K. (2016). Rapid photo-degradation of 2-chlorophenol under visible light irradiation using cobalt oxide-loaded TiO_2/reduced graphene oxide nanocomposite from aqueous media. *Journal of Environmental Management*, 165, 1–10. DOI: 10.1016/j.jenvman.2015.09.013.

[31] Ma, H., Zhang, J., Wang, M., Sun, S. (2019). Modification of Y-Zeolite with Zirconium for Enhancing the Active Component Loading: Preparation and Sulfate Adsorption Performance of $ZrO(OH)_2$/Y-Zeolite. *ChemistrySelect*, 4 (27), 7981–7990. DOI: 10.1002/slct.201901519.

[32] Fu, H., Zhong, L., Yu, Z., Liu, W., Abdel-Fatah, M.A., Li, J., Mingzhang, Yu, J., Dong, W., Lee, S.S. (2022). Enhanced adsorptive removal of ammonium on the Na^+/Al^{3+} enriched natural zeolite. *Separation and Purification Technology*, 298 (April), 121507. DOI: 10.1016/j.seppur.2022.121507.

[33] Mehdi, B., Belkacemi, H., Brahmi-Ingrachen, D., Braham, L.A., Muhr, L. (2022). Study of nickel adsorption on NaCl-modified natural zeolite using response surface methodology and kinetics modeling. *Groundwater for Sustainable Development*, 17(March), 100757. DOI: 10.1016/j.gsd.2022.100757.

[34] Bendou, S., Amrani, M. (2014). Effect of Hydrochloric Acid on the Structural of Sodic-Bentonite Clay. *Journal of Minerals and Materials Characterization and Engineering*, 02 (05), 404–413. DOI: 10.4236/jmmce.2014.25045.

[35] Susi, E.P., Wijaya, K., Wangsa, Pratika, R.A., Hariani, P.L. (2020). Effect of nickel concentration in natural zeolite as catalyst in hydrocracking process of used cooking oil. *Asian Journal of Chemistry*, 32(11), 2773–2777. DOI: 10.14233/ajchem.2020.22708.

[36] Zendelska, A., Golomeova, M., Jakupi, Š., Lisičkov, K., Kuvendžiev, S., Marinkovski, M. (2018). Characterization and application of clinoptilolite for removal of heavy metal ions from water resources. *Geologica Macedonica*, 32(1), 21–32.

[37] Byrappa, K., Kumar, B.V.S. (2007). Characterization of zeolites by infrared spectroscopy. *Asian Journal of Chemistry*, 19(6), 4933–4935.

[38] Nallusamy, S., Sujatha, K. (2020). Experimental analysis of nanoparticles with cobalt oxide synthesized by coprecipitation method on electrochemical biosensor using FTIR and TEM. *Materials Today: Proceedings*, 37(Part 2), 728–732. DOI: 10.1016/j.matpr.2020.05.735.

[39] Lee, S.K., Lee, U.H., Hwang, Y.K., Chang, J.S., Han Jang, N. (2019). Catalytic and sorption applications of porous nickel phosphate materials. *Catalysis Today*, 324(March 2018), 154–166. DOI: 10.1016/j.cattod.2018.06.012.

[40] Vifttaria, M., Nurhayati, N., Anita, S. (2019). Surface Acidity of Sulfuric Acid Activated Maredan Clay Catalysts with Boehm Titration Method and Pyridine Adsorption-FTIR. *Journal of Physics: Conference Series*, 1351(1) DOI: 10.1088/1742-6596/1351/1/012040.

[41] Rinaldi, N., Kristiani, A. (2017). Physicochemical of pillared clays prepared by several metal oxides. *AIP Conference Proceedings*, 1823(March). DOI: 10.1063/1.4978136.

[42] Zholobenko, V., Freitas, C., Jendrlin, M., Bazin, P., Travert, A., Thibault-Starzyk, F. (2020). Probing the acid sites of zeolites with pyridine: Quantitative AGIR measurements of the molar absorption coefficients. *Journal of Catalysis*, 385, 52–60. DOI: 10.1016/j.jcat.2020.03.003.

[43] Putri, Q.U., Hasanudin, H., Asri, W.R. (2023). Production of levulinic acid from glucose using nickel phosphate - silica catalyst. *Reaction Kinetics, Mechanisms and Catalysis*, 136(1), 287–309. DOI: 10.1007/s11144-022-02334-3.

[44] Hasanudin, H., Asri, W.R., Said, M., Hidayati, P.T., Purwaningrum, W., Novia, N., Wijaya, K. (2022). Hydrocracking optimization of palm oil to bio-gasoline and bio-aviation fuels using molybdenum nitride-bentonite catalyst. *RSC Advances*, 12(26), 16431–16443. DOI: 10.1039/D2RA02438A.

[45] Wijaya, K., Nadia, A., Dinana, A., Pratiwi, A.F., Tikoalu, A.D., Wibowo, A.C. (2021). Catalytic hydrocracking of fresh and waste frying oil over Ni-and Mo-based catalysts supported on sulfated silica for biogasoline production. *Catalysts*, 11 (10), 1150. DOI: 10.3390/catal11101150.

[46] Saab, R., Polychronopoulou, K., Anjum, D.H., Charisiou, N.D., Goula, M.A., Hinder, S.J., Baker, M.A., Schiffer, A. (2022). Effect of SiO_2/Al_2O_3 ratio in Ni/Zeolite-Y and Ni-W/Zeolite-Y catalysts on hydrocracking of heptane. *Molecular Catalysis*, 528(April), 112484. DOI: 10.1016/j.mcat.2022.112484.

[47] Li, L., Wei, X.Y., Liu, G.H., Li, Z., Li, J.H., Liu, F.J., Kong, Q.Q., Fan, Z.C., Zong, Z.M., Bai, H.C. (2022). Selective catalytic hydroconversion of organic waster oil to cyclanes over a coal fly ash-derived zeolite-supported nickel catalyst: Waster to energy. *Fuel*, 316,123185. DOI: 10.1016/j.fuel.2022.123185.

[48] Pierella, L.B., Renzini, S., Anunziata, O.A. (2005). Catalytic degradation of high density polyethylene over microporous and mesoporous materials. *Microporous and Mesoporous Materials*, 81(1–3), 155–159. DOI: 10.1016/j.micromeso.2004.11.015.

[49] Cho, J.H., Park, J.H., Chang, T.S., Seo, G., Shin, C.H. (2012). Reductive amination of 2-propanol to monoisopropylamine over Co/γ-Al2O3 catalysts. *Applied Catalysis A: General*, 417–418, 313–319. DOI: 10.1016/j.apcata.2012.01.011.

[50] Argyle, M.D., Bartholomew, C.H. (2015). Heterogeneous catalyst deactivation and regeneration: A review. *Catalysts*, 5(1), 145–269. DOI: 10.3390/catal5010145.

[51] Turek, W., Haber, J., Krowiak, A. (2005). Dehydration of isopropyl alcohol used as an indicator of the type and strength of catalyst acid centres. *Applied Surface Science*, 252(3), 823–827. DOI: 10.1016/j.apsusc.2005.02.059.

[52] Min, H.K., Kim, Y.W., Kim, C., Ibrahim, I.A.M., Han, J.W., Suh, Y.W., Jung, K.D., Park, M.B., Shin, C.H. (2022). Phase transformation of ZrO_2 by Si incorporation and catalytic activity for isopropyl alcohol dehydration and dehydrogenation. *Chemical Engineering Journal*, 428(August 2021), 131766. DOI: 10.1016/j.cej.2021.131766.

[53] Hasanudin, H., Asri, W.R., Andini, L., Riyanti, F., Mara, A., Hadiah, F., Fanani, Z. (2022). Enhanced Isopropyl Alcohol Conversion over Acidic Nickel Phosphate-Supported Zeolite Catalysts. *ACS Omega*, 7(43), 38923–38932. DOI: 10.1021/acsomega.2c04647